Title	Topology optimization of damping material for reducing resonance response based on complex dynamic compliance
Auther(s)	Takezawa, Akihiro; Daifuku, Masafumi; Nakano, Youhei; Nakagawa, Kohya; Yamamoto, Takashi; Kitamura, Mitsuru
Citation	Journal of Sound and Vibration , 365 : 230 - 243
Issue Date	2016-03-17
DOI	10.1016/j.jsv.2015.11.045
Self DOI	
URL	http://ir.lib.hiroshima-u.ac.jp/00041267
Right	Copyright (c) 2015 ElsevierLtd. All rights reserved.
Relation	

Topology optimization of damping material for reducing resonance response based on complex dynamic compliance

Akihiro Takezawa[a,*], Masafumi Daifuku[b], Youhei Nakano[b], Kohya Nakagawa[c], Takashi Yamamoto[d], Mitsuru Kitamura[a]

[a] *Division of Mechanical Systems and Applied Mechanics, Institute of Engineering, Hiroshima University, 1-4-1 Kagamiyama, Higashi-Hiroshima, Hiroshima, Japan*
[b] *Department of Transportation and Environmental Engineering, Graduate School of Engineering, Hiroshima University, 1-4-1 Kagamiyama, Higashi-Hiroshima, Hiroshima, Japan*
[c] *Technical Research Center, Mazda Motor Corporation, 3-1, Shin-chi, Fuchu-cho, Aki-gun, Hiroshima, Japan*
[d] *Department of Mechanical Engineering, Kogakuin University, 2665-1 Nakano, Hachioji, Tokyo, Japan*

Abstract

In this research, we propose a new objective function for optimizing damping materials to reduce the resonance peak response in the frequency response problem, which cannot be achieved using existing criteria. The dynamic compliance in the frequency response problem is formulated as the scalar product of the conjugate transpose of the amplitude vector and the force vector of the loading nodes. The proposed objective function methodology is implemented using the common solid isotropic material with penalization (SIMP)

*Corresponding author. Tel: +81-82-424-7544; Fax: +81-82-422-7194
Email addresses: akihiro@hiroshima-u.ac.jp (Akihiro Takezawa), m130657@hiroshima-u.ac.jp (Masafumi Daifuku), m146372@hiroshima-u.ac.jp (Youhei Nakano), nakagawa.ko@mazda.co.jp (Kohya Nakagawa), takashi_yamamoto@cc.kogakuin.ac.jp (Takashi Yamamoto), kitamura@hiroshima-u.ac.jp (Mitsuru Kitamura)

method for topology optimization. The optimization problem is formulated as maximizing the complex part of the proposed complex dynamic compliance under a volume constraint. 2D and 3D numerical examples of optimizing the distribution of the damping material on the host structure are provided to illustrate the validity and utility of the proposed methodology. In these numerical studies, the proposed objective function worked well for reducing the response peak in both lower and upper excitation frequencies around the resonance. By adjusting the excitation frequency, multi-resonance peak reduction may be achieved with a single frequency excitation optimization.
Keywords: , Damping material, Optimal design, Topology optimization, Sensitivity analysis, Finite element method

1. INTRODUCTION

Suppressing vibrations is one of the most important performance factors for mechanical devices subject to dynamic forces. Using damping materials is an important solution for this issue, and is especially effective for reducing the response peak. For example, sheet-like damping materials are often laid over metal plates in vehicle bodies to reduce the response to external loads. However, increasing the amount of damping material reduces the cost-effectiveness and increases the weight of the devices. Thus, there is growing demand for optimizing the shape and layout of damping materials.

Various methodologies for optimizing damping materials have been proposed. One of the early works on such optimization is the theoretical and experimental study of damping material layout for plates and beams by Plunkett and Lee [1]. Numerical analysis, such as the finite element method

(FEM), have been introduced for accurate analysis and detailed optimization in recent research. Chen and Huang [2] studied location and thickness optimization for damping materials based on a topographical optimization method. Zheng and Tan [3] also studied location and thickness optimization for damping materials using a genetic algorithm. They extended this methodology to optimization of damping material layout on cylindrical shells [4]. Although these researches are limited to location optimization for a fixed shape of the damping material, some papers have studied distribution optimization of damping materials. Alvelid [5] proposed an original gradient-based method, while Chia et al. [6] used cellular automata to study this issue.

Topology optimization (TO) [7, 8] is a methodology that achieves detailed optimization of device shapes, and has led to significant improvements in vibration characteristics of structures. Both maximization of the eigenfrequency [9, 10, 11, 12] and reduction of the response in the frequency response problem [13, 14, 15, 16] have been studied. However, these studies ignore the damping effect, whereas an optimization methodology for damping material distribution on a host plate has recently been proposed. Ling et al. [17] developed an optimization to maximize the modal loss factor based on eigenfrequency analysis. Kang et al. [18] proposed an optimization methodology based on frequency response analysis. They also extended their work to simultaneous optimization of the damping and host layers [19]. An experimental verification of these works has also been reported [20]. Fang and Zheng [21] studied the effect of modal sensitivity analysis on optimization of the damping material. Moreover, TO has been further extended to transient

response optimization [22] and mode shape optimization [23, 24].

Of these approaches, we focus on frequency response-based optimization, which is more straightforward than the eigenfrequency-based method when the excitation frequency can be predicted. A typical objective function proposed in previous research is minimization of the amplitude of the loading domain [18, 19, 21]. However, in actual mechanical design, the damping material is usually used to reduce the response peak at resonance near the excitation frequency rather than the response under the specified single frequency. Because the response amplitude is decided by the mutual effect of the mass, stiffness and damping of the vibration system while the response peak is affected only by damping in theory, the optimal solution obtained from this objective function will not always work well for peak reduction. Thus, an alternative criterion for the damping effect that can be used as an objective function in the peak reduction design problem is required.

On the other hand, the dynamic compliance proposed by Ma et al. [13, 16, 25], which was originally the scalar product of the force and amplitude vectors, is an effective objective function for optimization of non-damped structures. The advantage of dynamic compliance is that its sensitivity can be calculated without solving the adjoint equation as with static compliance [8]. Jog [26] re-defined dynamic compliance as the energy dissipated per cycle through damping. Although peak reduction optimization was not studied in this paper, the objective function can be used for this issue because it directly represents the damping effect.

Based on this research, we introduce a new objective function for optimizing damping material distribution on a host structure in peak reduction

optimization by extending the original dynamic compliance into complex space. This paper is organized as follows. The complex dynamic compliance is first formulated as a criterion for the damping effect based on a discrete vibration system subject to a dynamic force. The proposed objective function is implemented using the solid isotropic material with penalization (SIMP) method for TO. The relationship between the physical properties of the material and the density function is defined. The optimization problem is then formulated as maximizing the complex part of the proposed complex dynamic compliance under a volume constraint. The optimization algorithm is constructed using the method of moving asymptotes (MMA) [27] as an optimizer. We finally provide 2D and 3D numerical examples to illustrate the validity and utility of the proposed methodology.

2. Criteria for damping effect

2.1. Design objective

Let us consider a vibration problem involving a thin plate structure composed of a host layer Ω_h and a damping layer Ω_d as shown in Fig. 1. The design target is optimal distribution of the damping materials in a damping layer on the fixed host layer. The damping and host layers are modeled as damped and undamped linear elastic bodies, respectively. The hysteretic damping model is introduced for the damping material. Thus, the stiffness of the material E_d including the damping effect is formulated as follows:

$$E_d = E_{do}(1 + i\eta), \tag{1}$$

where E_{do} and η are the Young's modulus and the loss factor of the material respectively. This forced vibration problem is analyzed by the FEM. When

the whole structure is discretized into a discrete system with n degrees of freedom (DOFs), the equations of motion for the structure with an external dynamic force $\mathbf{l}$ is formulated as follows:

$$\mathbf{M}\ddot{\mathbf{z}} + \mathbf{K}\mathbf{z} = \mathbf{l}, \tag{2}$$

where $\mathbf{M}$ and $\mathbf{K}$ are the mass and stiffness matrices respectively, and $\mathbf{z}$ is the complex displacement vector. The stiffness matrix $\mathbf{K}$ is composed of a real part $\mathbf{K}_r$ and an imaginary part $\mathbf{K}_i$, so that $\mathbf{K} = \mathbf{K}_r + i\mathbf{K}_i$. Let us consider the case of a complex dynamic load $\mathbf{l} = \mathbf{f}e^{i\omega t}$ applied to the structure, where $\mathbf{f}$ and ω are the load amplitude and angular frequency. Assuming that the periodic response is $\mathbf{z} = \mathbf{u}e^{i\omega t}$, where $\mathbf{u} = [u_1, ...u_n]^T, u_j = u_{rj} + iu_{ij}$ is the complex amplitude with real parts u_{rj} and imaginary parts u_{ij}, and replacing $\mathbf{K}_i$ by the equivalent viscous damping matrix $\mathbf{C} = \mathbf{K}_i/\omega$, Eq.(2) may be represented as follows:

$$-\omega^2\mathbf{M}\mathbf{u} + i\omega\mathbf{C}\mathbf{u} + \mathbf{K}_r\mathbf{u} = \mathbf{f}. \tag{3}$$

We assume that the above equation has a unique solution $\mathbf{u}$ that avoids the repeated eigenvalue issue.

The energy W_d dissipated per cycle through damping is calculated as the integral of the scalar product of the damping force and the infinitesimal

displacement vector as follows:

$$\begin{aligned} W_d &= \int_{\text{Cycle}} \text{Re}(\mathbf{C}\dot{\mathbf{z}})^T \text{Re}(\mathrm{d}\mathbf{z}) = \int_0^{2\pi/\omega} \text{Re}(\dot{\mathbf{z}})^T \mathbf{C} \text{Re}(\dot{\mathbf{z}}) \mathrm{d}t \\ &= \int_0^{2\pi/\omega} \omega^2 [-u_{r1} \sin\omega t - u_{i1} \cos\omega t, ..., -u_{rn} \sin\omega t - u_{in} \cos\omega t] \mathbf{C} \\ &\qquad \cdot [-u_{r1} \sin\omega t - u_{i1} \cos\omega t, ..., -u_{rn} \sin\omega t - u_{in} \cos\omega t]^T \mathrm{d}t \\ &= \pi\omega \mathbf{u}^* \mathbf{C} \mathbf{u}, \end{aligned} \tag{4}$$

where $\text{Re}(\cdot)$ indicates the real part of a number, and the superscript $*$ indicates the conjugate transpose. In this research, considering that the response can be decreased by increasing the energy W_d dissipated by damping, maximizing W_d is set as the design objective.

Figure 1 is about here.

2.2. Complex dynamic compliance

The dynamic compliance proposed by Ma et al. [13] and calculated as the scalar product of the excitation force vector and the displacement vector is one of the basic criteria in the vibration optimization problem. However, their original work ignored damping and few subsequent studies have extended it in terms of the damping effect. Thus, we generalize dynamic compliance to handle the damping effect. First, let us multiply on the left by the complex conjugate transpose of the amplitude vector $\mathbf{u}^*$ in Eq.(3) as follows:

$$-\omega^2 \mathbf{u}^* \mathbf{M} \mathbf{u} + i\omega \mathbf{u}^* \mathbf{C} \mathbf{u} + \mathbf{u}^* \mathbf{K}_r \mathbf{u} = \mathbf{u}^* \mathbf{f}. \tag{5}$$

We define the right side of Eq.(5) as the complex dynamic compliance, so that $l_d = \mathbf{u}^*\mathbf{f}$. Of the three matrices in Eq. (5), the mass matrix $\mathbf{M}$ is positive definite and the real part of the stiffness matrix $\mathbf{K}_r$ and the equivalent viscous damping matrix $\mathbf{C} = \mathbf{K}_i/\omega = \eta\mathbf{K}_r/\omega$ are both positive semidefinite. Because the complex quadratic forms for positive definite and positive semidefinite matrices must be positive and non-negative real numbers respectively, $\mathbf{u}^*\mathbf{M}\mathbf{u}$, $\mathbf{u}^*\mathbf{K}_r\mathbf{u}$ and $\mathbf{u}^*\mathbf{K}_i\mathbf{u}$ are all real numbers. Thus, the following relationships can be obtained:

$$\mathrm{Re}(l_d) = -\omega^2\mathbf{u}^*\mathbf{M}\mathbf{u} + \mathbf{u}^*\mathbf{K}_r\mathbf{u}, \tag{6}$$

$$\mathrm{Im}(l_d) = \omega\mathbf{u}^*\mathbf{C}\mathbf{u}, \tag{7}$$

where $\mathrm{Im}(\cdot)$ indicates the imaginary part of a number. Comparing Eqs.(4) and (7), the energy W_d dissipated by damping can be maximized by maximizing the imaginary part $\mathrm{Im}(l_d)$ of the proposed complex dynamic compliance.

Note that, because the damping matrix $\mathbf{C}$ is always positive semidefinite even for the general viscous damping problem, the above discussion can also be applied to the general viscous damping problem.

Furthermore, when there is no damping in the system, $\mathrm{Re}(l_d)$ is equal to the original dynamic compliance [13]. When the force vector $\mathbf{f}$ is a real number vector, that is, no phase difference is considered in the excitation periodic load, $\mathrm{Im}(l_d)$ is equal to the dynamic compliance proposed by Jog [26].

3. Formulation of optimization methodology

3.1. Topology optimization

The TO method is used to optimize the damping material distribution in the damping layer Ω_d, because this method can perform fundamental optimization over domains with arbitrary shape and topology, including those with holes. The fundamental idea is to introduce a fixed, extended design domain D that includes *a priori* the optimal shape Ω_{opt}. The damping layer design Ω_d corresponds to the design domain D in this study. The material distribution in D is represented by the use of the following characteristic function:

$$\chi(\mathbf{x}) = \begin{cases} 1 & \text{if} \quad \mathbf{x} \in \Omega_{\text{opt}}, \\ 0 & \text{if} \quad \mathbf{x} \in D \setminus \Omega_{\text{opt}}. \end{cases} \tag{8}$$

Using this function, the material distribution problem in D is replaced by a material physical property χA distribution problem, where A is an arbitrary physical property of the original material of Ω_d. Unfortunately, the optimization problem does not have any optimal solutions [28]. A homogenization method is used to relax the solution space [7, 28]. In this way, the original material distribution optimization problem with respect to the characteristic function is replaced by an optimization problem for the "composite" consisting of the original material and a material with very low physical properties, mimicking holes with respect to the density function. This density function represents the volume fraction of the original material and can be regarded as a weak limit of the characteristic function. In the optimization problem, the relationship between the material properties of the composite and the density function must be defined. The most popular approach, which sets a penalized

proportional material property [29, 30], is the SIMP method. In this paper, the SIMP method is applied with relationships between the three material properties of the composite used in vibration analysis (Young's modulus E, mass density ρ and loss factor η) and the density function ϕ satisfying a simple equation involving the penalized material density:

$$E_{\text{eff}} = \phi^{p_E} E_{\text{o}}, \tag{9}$$

$$\rho_{\text{eff}} = \phi^{p_\rho} \rho_{\text{o}}, \tag{10}$$

$$\eta_{\text{eff}} = \phi^{p_\eta} \eta_{\text{o}}, \tag{11}$$

with

$$0 \leq \phi(\mathbf{x}) \leq 1, \ \mathbf{x} \in \Omega, \tag{12}$$

where the subscript eff signifies that the material property relates to the composite, the subscript o signifies that the material property relates to the original material, and p_E, p_ρ and p_η are positive penalization parameters. The above modeling is only introduced for the damping layer shown in Fig. 1 because the optimization target of this research is the distribution of the damping material on the fixed host layer.

3.2. Optimization problem

Based the damping effect criteria formulated above, we pose the optimization problem as the problem of maximizing the imaginary part of the complex dynamic compliance with an added volume constraint on the damping material:

$$\text{maximize}\, \text{Im}(l_d) = \omega \mathbf{u}^* \mathbf{C} \mathbf{u} = \mathbf{u}^* \mathbf{K}_i \mathbf{u}, \tag{13}$$

subject to

$$\text{Eq. (3)},$$

$$\int_{\Omega_d} \phi \mathrm{d}x \leq V_{\max}, \tag{14}$$

$$0 < \phi \leq 1, \tag{15}$$

where $V_{\max}$ is the allowable volume of the damping material.

3.3. Optimization algorithm

The optimization is performed using an algorithm that incorporates sensitivity calculations and updates the design variable using MMA [27]. To avoid element discontinuity and the mesh dependency problem in topology optimization, the so-called density filter, which averages the density of each element against the densities of neighborhood elements [31] is introduced. The optimization algorithm is presented in Fig. 2.

Figure 2 is about here.

3.4. Sensitivity analysis

To perform optimization, we use the MMA technique, which requires first-order sensitivity analysis of the objective function and constraints with respect to the design variable ϕ. Thus, we must derive the first-order sensitivity of the complex dynamic compliance.

We first introduce a Lagrangian, which is the sum of the dynamic compliance and a zero function which is the inner product of the complex conjugate

transpose of the vibration equation in Eq. (3) and a Lagrange multiplier $\widetilde{\mathbf{u}}$ as follows:

$$l = \mathbf{u}^*\mathbf{f} + \{\mathbf{u}^*(-\omega^2\mathbf{M} - i\omega\mathbf{C} + \mathbf{K}_r) - \mathbf{f}^*\}\widetilde{\mathbf{u}}. \tag{16}$$

The derivative of the Lagrangian with respect to the j-th design variable ϕ_j, which equals to the derivative of the objective function, is then obtained as follows:

$$\begin{aligned}\frac{\partial l}{\partial \phi_j} &= \frac{\partial \mathbf{u}^*}{\partial \phi_j}\mathbf{f} + \left\{\frac{\partial \mathbf{u}^*}{\partial \phi_j}(-\omega^2\mathbf{M} - i\omega\mathbf{C} + \mathbf{K}_r) + \mathbf{u}^*\left(-\omega^2\frac{\partial \mathbf{M}}{\partial \phi_j} - i\omega\frac{\partial \mathbf{C}}{\partial \phi_j} + \frac{\partial \mathbf{K}_r}{\partial \phi_j}\right)\right\}\widetilde{\mathbf{u}} \\ &= \frac{\partial \mathbf{u}^*}{\partial \phi_j}\left\{(-\omega^2\mathbf{M} - i\omega\mathbf{C} + \mathbf{K}_r)\widetilde{\mathbf{u}} + \mathbf{f}\right\} + \mathbf{u}^*\left(-\omega^2\frac{\partial \mathbf{M}}{\partial \phi_j} - i\omega\frac{\partial \mathbf{C}}{\partial \phi_j} + \frac{\partial \mathbf{K}_r}{\partial \phi_j}\right)\widetilde{\mathbf{u}}.\end{aligned} \tag{17}$$

When $\widetilde{\mathbf{u}} = -\bar{\mathbf{u}}$ and $\mathbf{f} = \bar{\mathbf{f}}$, where the overbar (-) indicates the conjugate, the first term is zero because it equals the conjugate of the vibration equation in Eq. (3). Finally, under the condition that the force vector $\mathbf{f}$ is a real number vector, the first-order sensitivity of the complex dynamic compliance is obtained as follows:

$$\frac{\partial l}{\partial \phi_j} = -\mathbf{u}^*\left(-\omega^2\frac{\partial \mathbf{M}}{\partial \phi_j} - i\omega\frac{\partial \mathbf{C}}{\partial \phi_j} + \frac{\partial \mathbf{K}_r}{\partial \phi_j}\right)\bar{\mathbf{u}}. \tag{18}$$

Deriving the first-order sensitivity of the complex dynamic compliance is thus the self-adjoint problem, as with the original dynamic compliance [13]. The first-order sensitivity of the objective function in Eq. (13) is easily obtained by taking the imaginary part of Eq. (18).

4. Numerical examples

4.1. Setting of penalization parameters

Several numerical examples are provided to confirm the validity and utility of the proposed methodology. Before studying the TO problem, the penalization parameters for the interpolated physical properties in Eqs. (9-11) are determined using a single DOF system imitating the density optimization of one element in the damping layer as shown in Fig. 3. The design variable is the single DOF system, while the mass, spring and damper are formulated as functions of the design variable ϕ: $k = \phi^{p_k} k_o$, $m = \phi^{p_m} m_o$ and $c = \phi^{p_\eta} \eta_o k/\omega = \eta^{p_k + p_\eta} k_o/\omega$. The values k_o, m_o and η_o are set to 1, 1 and 0.3 respectively. The frequency response problem for this system under the periodic excitation load $fe^{i\omega t}$ is considered using the periodic response $x = ue^{i\omega t}$, where f is set to 1.

First, the typical values of the penalty parameters p_k and p_m are 3 and 1 respectively in the existing vibration TO literature [11, 17, 18]. The reason behind this setting is that the angular eigenfrequency ω_n is then $\sqrt{k/m} = \sqrt{k_o/m_o}\phi$, which guarantees an increase in ω_n as ϕ increases in the interval $0 \leq \phi \leq 1$. It may also be possible to base the response reduction on the eigenfrequency shift. In this research, we base the response reduction not on the eigenfrequency shift but on the damping effect, which means that the variation of the eigenfrequency should be small according to the variation of the design variable. Thus, p_k and p_m are both set to the same value 3.

The penalization parameter p_η of the loss factor is then studied by introducing the complex dynamic compliance $u^* f$ into this single DOF system. Figure 4 shows the relationship between $\mathrm{Im}(u^* f)$ and ϕ ($0 \leq \phi \leq 1$) with pe-

nalizations $p_k = p_m = 3$ and $p_\eta = 1, 3, 6$ in the cases where $\omega = 0.5\omega_n = 0.5$ and $\omega = 1.5\omega_n = 1.5$. $\mathrm{Im}(u^* f)$ must be zero when $\phi = 0$ because these is no damping effect in that state. However, when $0 \leq p_\eta \leq 3$, $\mathrm{Im}(u^* f)$ approaches ∞ or some non-zero number as $\phi \to 0$ and $\mathrm{Im}(u^* f)$ is discontinuous at $\phi = 0$. When $3 < p_\eta$, this discontinuity problem is resolved. Based on the above, and also considering the penalization effect of the intermediate value of ϕ, p_η is set to 6 in the following numerical examples.

Moreover, as opposed to the original dynamic compliance calculated as uf without damping in this single DOF example, $\mathrm{Im}(u^* f)$ remains positive in the both the upper and lower frequencies of the eigenfrequency. That is, $\mathrm{Im}(u^* f)$ is positive even when the phase is opposite between the excitation load and the displacement of the loading point. Thus, this can be used as a general objective function independent of the phase difference between the excitation load and the displacement at the loading point.

Figures 3 and 4 are about here.

4.2. 2D cantilever example

A numerical example involving a 2D cantilever is provided first to confirm the validity of the proposed methodology. In this example, a 2D plane strain model is used to approximate a cantilever plate composed of host and damping layers with a dynamic line-distributed vertical excitation force of -0.1N/mm on the bottom edge of the right side as shown in Fig. 5. The material of the host layer is assumed to be aluminum with a Young's modulus

of 70 GPa, a Poisson's ratio of 0.3 and a mass density of 2.7×10^3 kg/m^3. The damping material is assumed to be one used in automotive bodies with a Young's modulus of 1 GPa, a Poisson's ratio of 0.4, a mass density of 1×10^3 kg/m^3 and a loss factor of 0.3. The optimization problem in Eqs. (13-15) is solved according to the algorithm set out in Fig. 2. At each iteration, we perform a finite element analysis of the vibration equation and a single update of the design variables. The upper limit constraining the volume of the damping material in Eq. (14) is set to 60% of the full volume of the damping layer. The initial value of the design variable is set uniformly to 0.6. All finite element analyses are performed using the commercial software COMSOL Multiphysics for quick implementation of the proposed methodology and to effectively solve the vibration equations with a multi-core processor. The domain is discretized using 1 mm $\times$ 1 mm square second-order Lagrange finite elements.

Figure 5 is about here.

As a reference model for optimization, we consider the fully-covered (FC) plate where the damping material is 3/5 the thickness of the damping layer shown in Fig. 5. The total volume of the damping material is then the same as the upper limit on the volume. The first, second and third eigenfrequencies of the structure are 5.1 Hz, 32.0 Hz and 89.2 Hz, respectively. We also confirmed the same eigenfrequencies were obtained using 2 mm $\times$ 2 mm and 0.5 mm $\times$ 0.5 mm square second-order Lagrange finite elements.

To reduce the resonance peak at the first, second and third eigenfrequencies, we set the excitation vibration frequencies to 2 Hz, 8 Hz, 26 Hz, 42 Hz, 80 Hz and 100 Hz. These are used as the lower and upper frequencies for each eigenfrequency. In addition to the maximizing the imaginary part of the dynamic compliance (abbreviated as IDC hereafter) in Eq. (13), we also minimize the amplitude of the loading point (abbreviated as AMP hereafter), which is a typical objective function in damping material optimization based on frequency response [18, 19].

The convergence history of the IDC in maximizing the IDC under 2 Hz and 8 Hz excitations is shown in Fig. 6 to confirm smooth convergence. Figures 7-9 show the optimal results for each eigenfrequency after 50 iterations, including the optimal configurations, a comparison of IDC with the initial and FC plate results, and a comparison of the amplitude of the loading point with the FC plate and amplitude minimization results. The results in Figs. 7 (a), (b) and (c) are almost the same because the damping material on the left side contributes to increased energy loss due to damping and to amplitude reduction due to stiffness. However, (d) is quite different because the excitation frequency is greater than the first eigenfrequency so the optimizer decreases the first eigenfrequency to reduce the response amplitude under the 8 Hz excitation. From Figs. 7 (e) and (f), because the IDC and AMP perform better than the initial and the FC plate at each excitation frequency, they may both succeed in optimization. However, as shown in Fig. 7 (f), only the IDC criterion successfully reduces the peak amplitude.

Note that, in Fig. 7 (e), the initial and FC plates attained higher IDC values than the optimum in the frequency ranges of 5.3 Hz to 5.4 Hz and

of 4.1 Hz to 5.3 Hz, respectively. That is, the IDC for the initial and FC plates can have better objective functions than the optimal solutions in the neighborhood of the resonance frequency, contrary to what is observed in other regions. In this frequency range, a local optimum that is inferior at reducing the response peak could be generated. Thus, we need to use an excitation frequency that is not close to the resonant frequency. This also indicates an initial dependency in the proposed method. If the resonant frequency of the initial guess is close to the excitation frequency, then the proposed methodology does not work well. Thus, the initial guess should be a shape having resonant frequencies close to the optimal solution's ones.

The discussion above can also be applied to the solution around second- and third-order eigenfrequencies. The only difference is that the layout of the damping material fails in the AMP optimization for lower frequency excitations. As shown in Fig. 8, damping material decreases the second and third eigenfrequencies because of its mass. Thus, removing the damping material may be optimal under a single excitation frequency near under the second or third eigenfrequency. In these frequency domains, only IDC maximization provides effective solutions for reducing the response peak.

Figures 6, 7, 8 and 9 are about here.

4.3. 3D plate example

Our second numerical example, shown in Fig. 10, involves optimizing the layout of damping material over a 3D host plate. A dynamic line-distributed

vertical excitation force of 1N/mm is applied to the right bottom edge of the host plate.

The materials in the damping and host layers are the same as in the previous example. The upper limit on the volume of damping material in Eq. (14) is set to 50% of the volume of the damping layer. The initial value of the design variable is set uniformly to 0.5. The domain is discretized using 4 mm $\times$ 4 mm $\times$ 2 mm cuboid second-order Lagrange finite elements. The design variable is set to be a 2 mm $\times$ 2 mm $\times$ 2 mm cubic mesh on the damping layer based on the concept of multi-resolution TO [32].

Figure 10 is about here.

An FC plate with damping material half the thickness of the design domain is considered as a reference model for 3D optimization. Figure 11 shows the integral of the amplitude of the loading point under a force with a frequency of 0-50 Hz. Mode shapes at the response peaks are also shown. In the above frequency range, there were no repeated eigenvalues and all responses were obtained uniquely. The response peaks are observed at 2.2 Hz, 13.9 Hz, 34.6 Hz and 40.0 Hz. We also confirmed that similar eigenfrequencies within 0.2 Hz errors were obtained using 8 mm $\times$ 8 mm $\times$ 2 mm and 2 mm $\times$ 2 mm $\times$ 1 mm cuboid second-order Lagrange finite elements. To reduce these response peaks, we use excitation frequencies of 1 Hz, 12 Hz and 38 Hz. In particular, the last excitation frequency is chosen to reduce the third and fourth response peaks simultaneously.

Figure 11 is about here.

Figures 12-14 show the optimal solutions including the optimal configuration, deformation, IDC and AMP around the resonance frequency. Although all optima should have upper and lower symmetry shapes, the resulting shapes were slightly asymmetric due to numerical errors. Notice that the damping material is arranged to cover the high strain part of the base plate in each vibration shape. Because the response peaks are lower than for the FC structure, the optimization succeeded in every case. In Fig. 14, the third and fourth mode responses were reduced even with single frequency excitation optimization.

Figures 12, 13 and 14 are about here.

5. Conclusions

We have derived a new objective function, namely the complex dynamic compliance, to use in damping material layout optimization on a host structure with the intention of reducing the response peak at resonances. The complex dynamic compliance was formulated as the scalar product of the conjugate transpose of the amplitude vector and the force vector. Its imaginary part represents the energy dissipation per cycle through damping. The proposed objective function was implemented using the SIMP method for TO by regarding the Young's modulus, the mass density and the loss factor

of the damping material as functions of the density function. We then confirmed that peak reduction optimization could be achieved by maximizing the imaginary part of the dynamic compliance.

The optimization was successful in 2D and 3D FEM analysis models. In particular, in the 3D problem, simultaneous reduction of two resonance peaks was achieved with a single excitation frequency. However, the proposed objective function should not be set too close to the resonance frequency, because dynamic compliance has its peak at the resonance frequency while inferior solutions can take better values than the optimal solution near resonance.

In further research, simultaneous topology optimization of the damping and host structures should be considered. In addition to resonance response reduction, specification of the resonance frequency is also a fundamental design factor for mechanical devices. This may be affected by the shape of the host structure rather than the shape of the damping layer. By integrating two criteria, the imaginary part of the dynamic compliance and the resonance frequency, a multi-phase topology optimization of the damping and host materials would be achieved for both increasing the damping effect and specifying a resonance frequency.

Acknowledgments

This research was partially supported by JSPS KAKENHI Grant Numbers 25820422 and 25630436.

[1] R. Plunkett, C. T. Lee, Length optimization for constrained viscoelastic

layer damping, The Journal of the Acoustical Society of America, 48 (1970) 150–161.

[2] Y. C. Chen, S. C. Huang, An optimal placement of CLD treatment for vibration suppression of plates, International Journal of Mechanical Sciences, 44 (8) (2002) 1801–1821.

[3] H. Zheng, C. Cai, X. M. Tan, Optimization of partial constrained layer damping treatment for vibrational energy minimization of vibrating beams, Computers & Structures, 82 (29) (2004) 2493–2507.

[4] H. Zheng, C. Cai, G. S. H. Pau, G. R. Liu, Minimizing vibration response of cylindrical shells through layout optimization of passive constrained layer damping treatments, Journal of Sound and Vibration, 279 (3) 739–756.

[5] M. Alvelid, Optimal position and shape of applied damping material, Journal of Sound and Vibration, 310 (4) (2008) 947–965.

[6] C. M. Chia, J. A. Rongong, K. Worden, Strategies for using cellular automata to locate constrained layer damping on vibrating structures, Journal of Sound and Vibration, 319 (1) (2009) 119–139.

[7] M. P. Bendsøe, N. Kikuchi, Generating optimal topologies in structural design using a homogenization method, Computer Methods in Applied Mechanics and Engineering, 71 (2) (1988) 197–224.

[8] M. P. Bendsøe, O. Sigmund, Topology Optimization: Theory, Methods, and Applications, Springer-Verlag, Berlin, 2003.

[9] A. R. Diaz, M. P. Bendsøe, Shape optimization of structures for multiple loading conditions using a homogenization method, Structural Optimization, 4 (1) (1992) 17–22.

[10] Z. D. Ma, N. Kikuchi, H. C. Cheng, Topological design for vibrating structures, Computer Methods in Applied Mechanics and Engineering, 121 (1-4) (1995) 259–280.

[11] N. L. Pedersen, Maximization of eigenvalues using topology optimization, Structural and Multidisciplinary Optimization, 20 (1) (2000) 2–11.

[12] Q. Xia, T. Shi, M. Y. Wang, A level set based shape and topology optimization method for maximizing the simple or repeated first eigenvalue of structure vibration, Structural and Multidisciplinary Optimization, 43 (4) (2011) 473–485.

[13] Z. D. Ma, N. Kikuchi, I. Hagiwara, Structural topology and shape optimization for a frequency response problem, Computational Mechanics, 13 (3) (1993) 157–174.

[14] D. Tcherniak, Topology optimization of resonating structures using SIMP method, International Journal for Numerical Methods in Engineering, 54 (11) (2002) 1605–1622.

[15] L. Shu, M. Y. Wang, Z. Fang, Z. Ma, P. Wei, Level set based structural topology optimization for minimizing frequency response, Journal of Sound and Vibration, 330 (24) (2011) 5820–5834.

[16] X. Yang, Y. Li, Topology optimization to minimize the dynamic compliance of a bi-material plate in a thermal environment, Structural and Multidisciplinary Optimization, 47 (3) (2013) 399–408.

[17] Z. Ling, X. Ronglu, W. Yi, A. El-Sabbagh, Topology optimization of constrained layer damping on plates using method of moving asymptote (MMA) approach, Shock and Vibration, 18 (1-2) (2011) 221–244.

[18] Z. Kang, X. Zhang, S. Jiang, G. Cheng, On topology optimization of damping layer in shell structures under harmonic excitations, Structural and Multidisciplinary Optimization, 46 (1) (2012) 51–67.

[19] X. Zhang, Z. Kang, Vibration suppression using integrated topology optimization of host structures and damping layers, Journal of Vibration and Control, doi:10.1177/1077546314528368.

[20] S. Y. Kim, C. K. Mechefske, I. Y. Kim, Optimal damping layout in a shell structure using topology optimization, Journal of Sound and Vibration, 332 (12) (2013) 2873–2883.

[21] Z. Fang, L. Zheng, Topology Optimization for Minimizing the Resonant Response of Plates with Constrained Layer Damping Treatment, Shock and Vibration, 2015 (2015), 376854 (11 pages).

[22] S. Min, N. Kikuchi, Y. C. Park, S. Kim, S. Chang, Optimal topology design of structures under dynamic loads, Structural Optimization, 17 (2) (1999) 208–218.

[23] Y. Maeda, S. Nishiwaki, K. Izui, M. Yoshimura, K. Matsui, K. Terada, Structural topology optimization of vibrating structures with specified

eigenfrequencies and eigenmode shapes, International Journal for Numerical Methods in Engineering, 67 (2006) 597–628.

[24] A. Takezawa, M. Kitamura, Sensitivity analysis and optimization of vibration modes in continuum systems, Journal of Sound and Vibration, 332 (2013) 1553–1566.

[25] X. Yang, Y. Li, Structural topology optimization on dynamic compliance at resonance frequency in thermal environments, Structural and Multidisciplinary Optimization, 49 (1) (2014) 81–91.

[26] C. S. Jog, Topology design of structures subjected to periodic loading, Journal of Sound and Vibration, 253 (3) (2002) 687–709.

[27] K. Svanberg, The method of moving asymptotes- a new method for structural optimization, International Journal for Numerical Methods in Engineering, 24 (2) (1987) 359–373.

[28] G. Allaire, Shape Optimization by the Homogenization Method, Springer-Verlag, New York, 2001.

[29] M. P. Bendsøe, Optimal shape design as a material distribution problem, Structural Optimization, 1 (4) (1989) 193–202.

[30] M. Zhou, G. I. N. Rozvany, The COC algorithm, Part II: Topological, geometrical and generalized shape optimization, Computer Methods in Applied Mechanics and Engineering, 89 (1-3) (1991) 309–336.

[31] T. E. Bruns, O. Sigmund, D. A. Tortorelli, Numerical methods for the topology optimization of structures that exhibit snap-through, Interna-

tional Journal for Numerical Methods in Engineering, 55 (10) (2002) 1215–1237.

[32] T. Nguyen, G. Paulino, J. Song, C. Le, A computational paradigm for multiresolution topology optimization (MTOP), Structural and Multidisciplinary Optimization, 41 (4) (2010) 525–539.

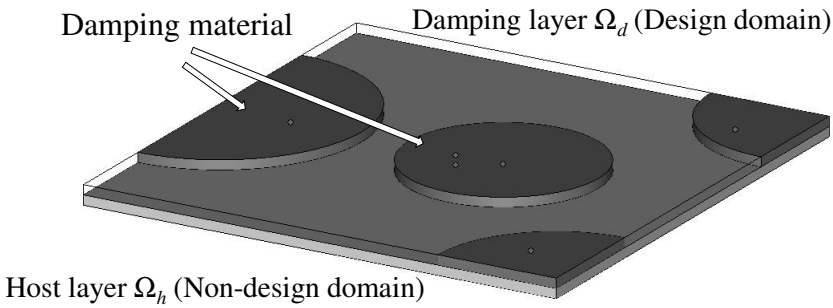

Figure 1: An outline of the design target structure composed of the damping and host layers.

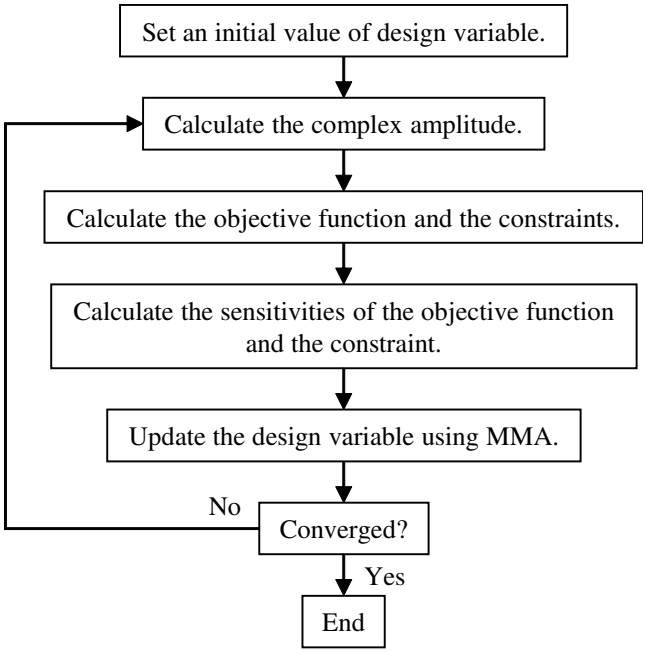

Figure 2: Flowchart of the optimization algorithm.

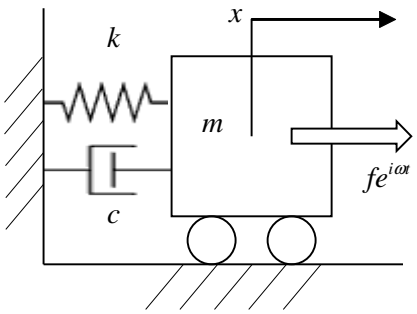

Figure 3: A single DOF system for deciding penalization parameters.

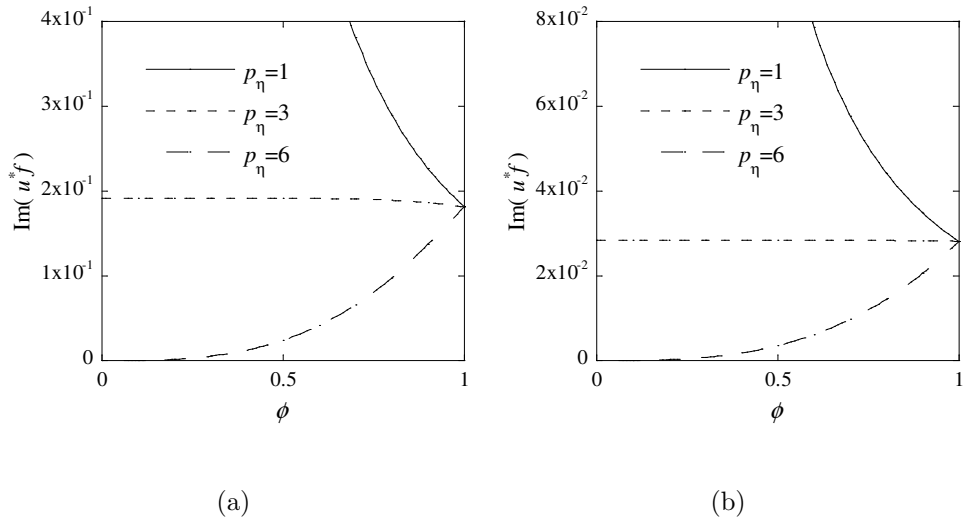

(a) (b)

Figure 4: Relationship between the design variable and the imaginary part of the complex dynamic compliance with (a) $\omega = 0.5\omega_n = 0.5$ and (b) $\omega = 1.5\omega_n = 1.5$.

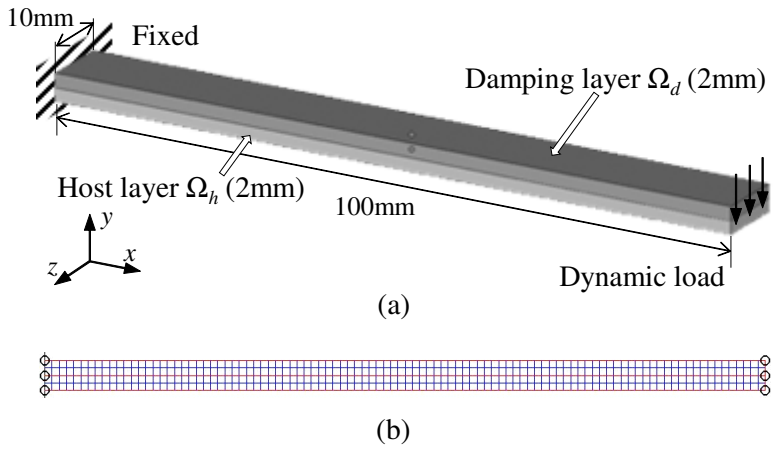

Figure 5: (a) Outline and (b) mesh discretization of the design domain for the 2D example.

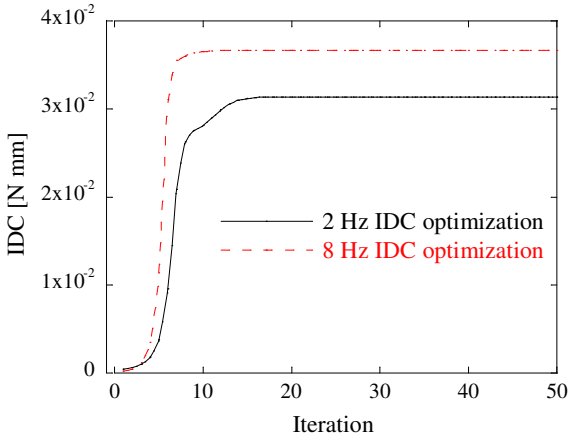

Figure 6: Convergence histories of IDC in maximizing the IDC under 2 Hz and 8 Hz excitations.

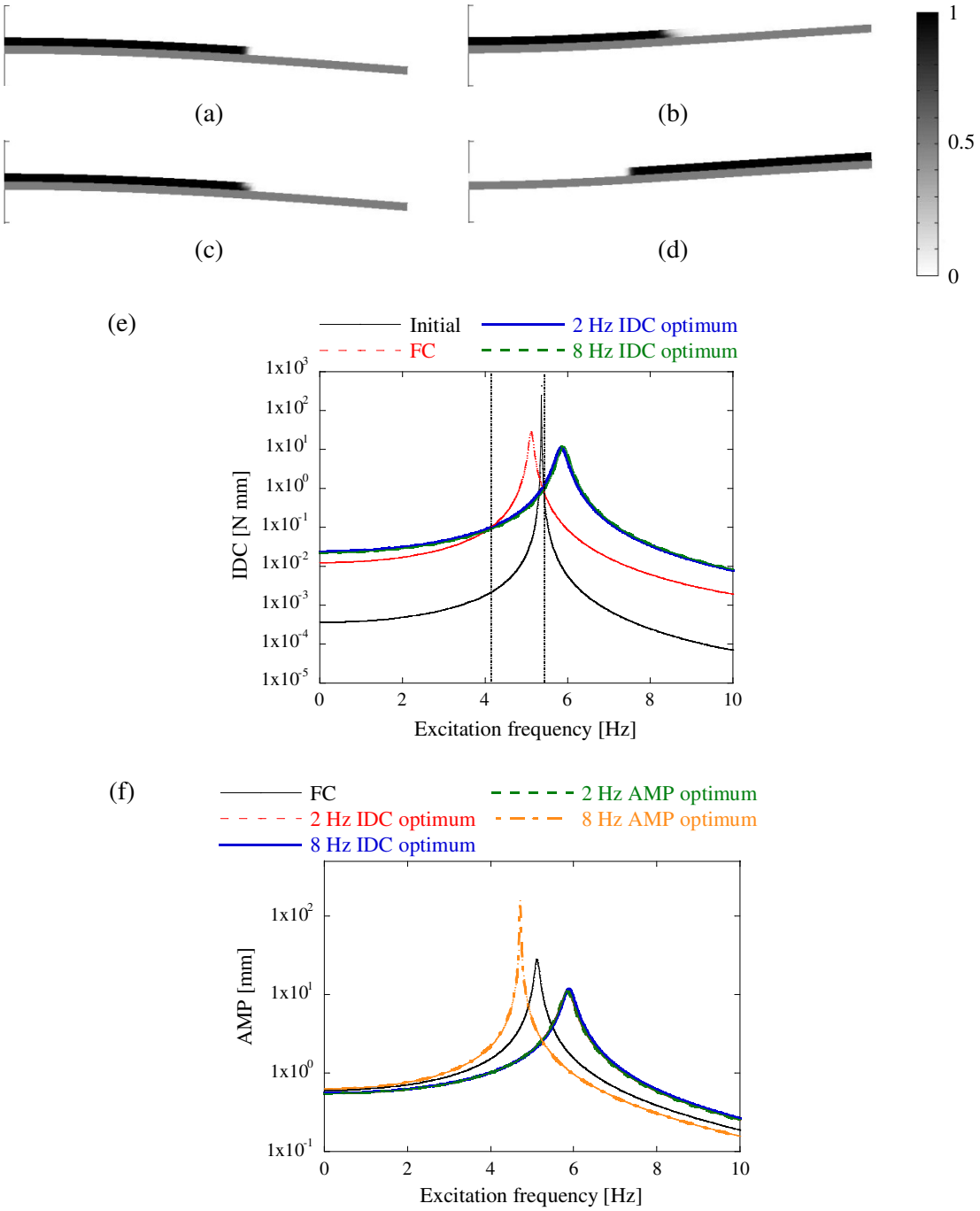

Figure 7: Optimal results for reducing the first mode resonance response. (a)-(d): Optimal configuration of the damping layer plotted by gray scale. (The host layer is shown in gray beneath the damping layer.) (a): Maximization of IDC under 2 Hz excitation. (b): Maximization of IDC under 8 Hz excitation. (c): Minimization of AMP under 2 Hz excitation. (d): Minimization of AMP under 8 Hz excitation. (e): Comparison of IDC in the 0-10 Hz excitation frequency range with 0.01 Hz resolution. The broken black lines indicate the frequency range where the initial or FC plates attained higher IDC values than the optimal configuration. (f): Comparison of AMP in the 0-10 Hz excitation frequency range with 0.01 Hz resolution. In (e) and (f), the results of maximization of IDC at 2 Hz and 8 Hz and minimization of AMP at 2 Hz overlap.

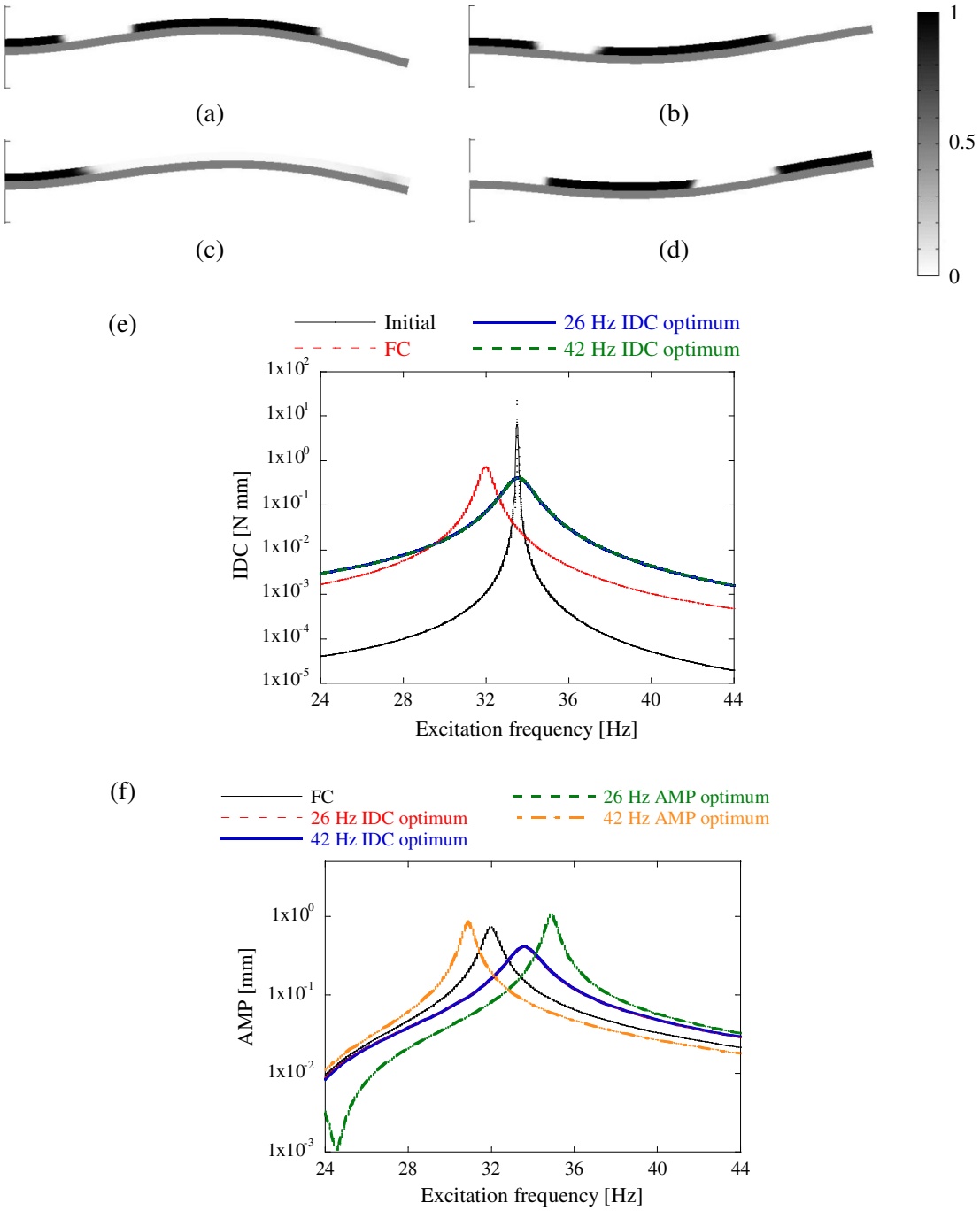

Figure 8: Optimal results for reducing the first mode resonance response. (a)-(d): Optimal configuration of the damping layer plotted by gray scale. (The host layer is shown in gray beneath the damping layer.) (a): Maximization of IDC under 26 Hz excitation. (b): Maximization of IDC under 42 Hz excitation. (c): Minimization of AMP under 26 Hz excitation. (d): Minimization of AMP under 42 Hz excitation. (e): Comparison of IDC in the 24-44 Hz excitation frequency range with 0.01 Hz resolution. (f): Comparison of AMP in the 24-44 Hz excitation frequency range with 0.01Hz resolution. In (e) and (f), the results of maximization of IDC at 26 Hz and 42 Hz overlap.

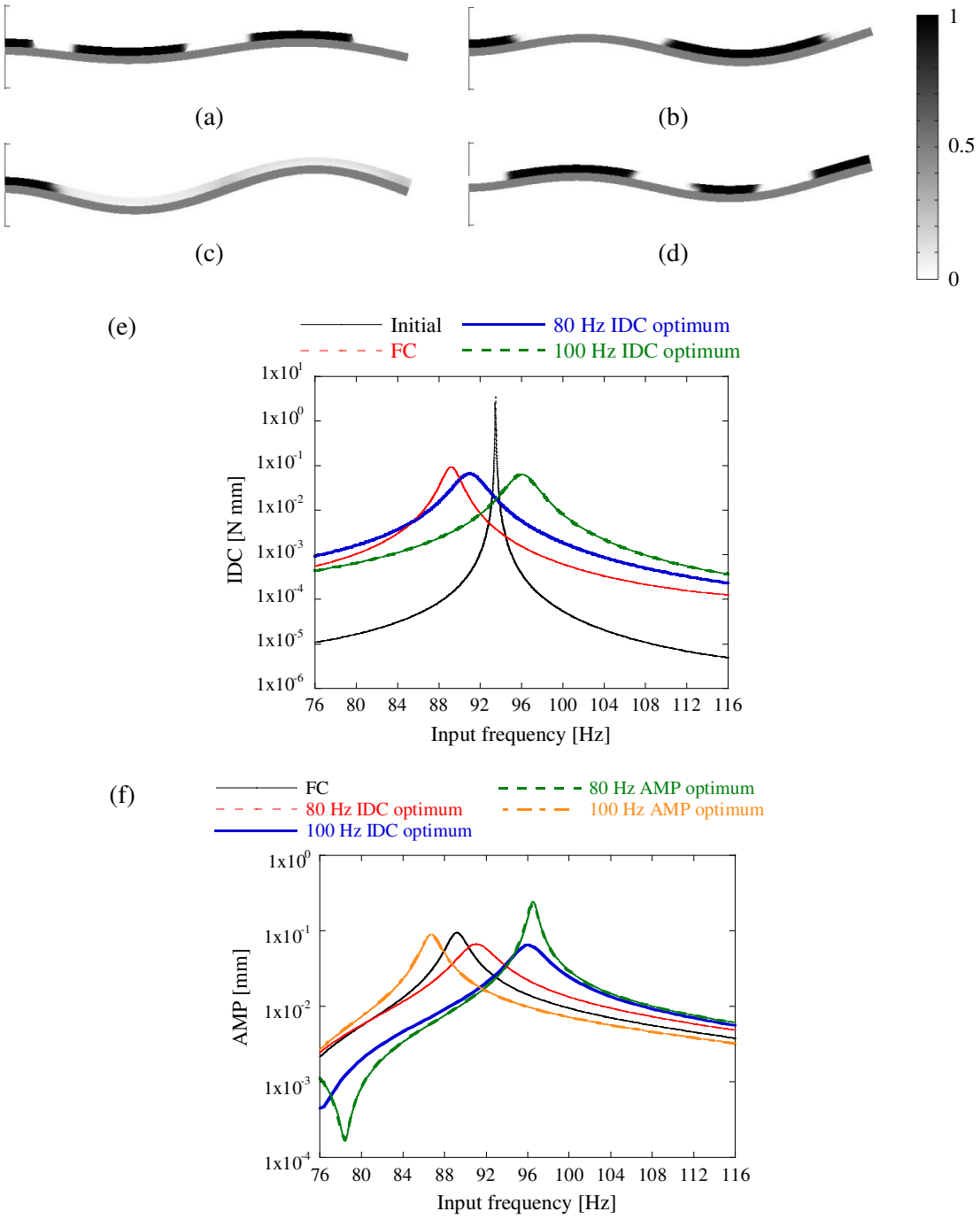

Figure 9: Optimal results for reducing the first mode resonance response. (a)-(d): Optimal configuration of the damping layer plotted by gray scale. (The host layer is shown in gray beneath the damping layer.) (a): Maximization of IDC under 80 Hz excitation. (b): Maximization of IDC under 100 Hz excitation. (c): Minimization of AMP under 80 Hz excitation. (d): Minimization of AMP under 100 Hz excitation. (e): Comparison of IDC in the 76-116 Hz excitation frequency range with 0.01 Hz resolution. (f): Comparison of AMP in the 76-116 Hz excitation frequency range with 0.01 Hz resolution.

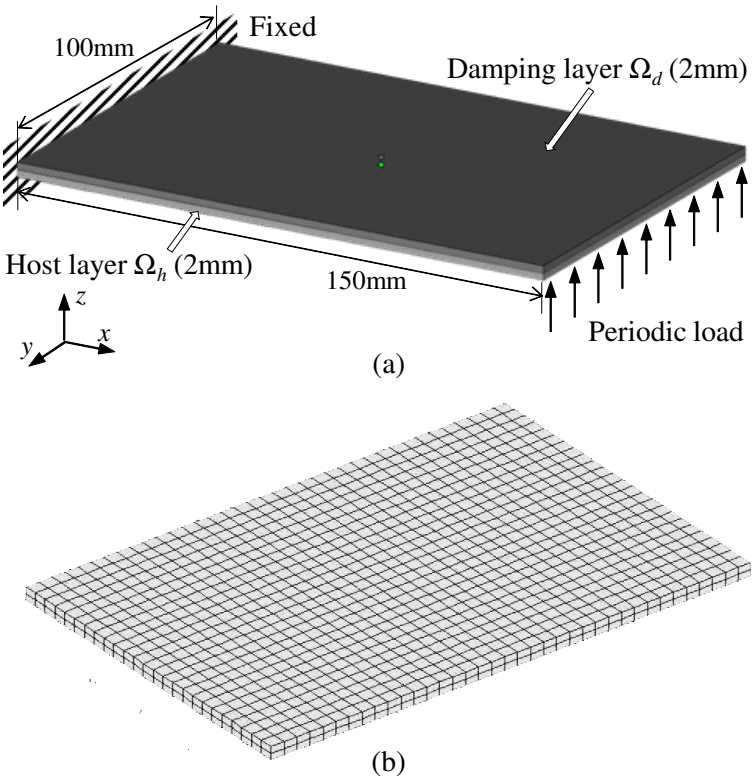

Figure 10: (a) Outline and (b) mesh discretization of the design domain of the 3D example.

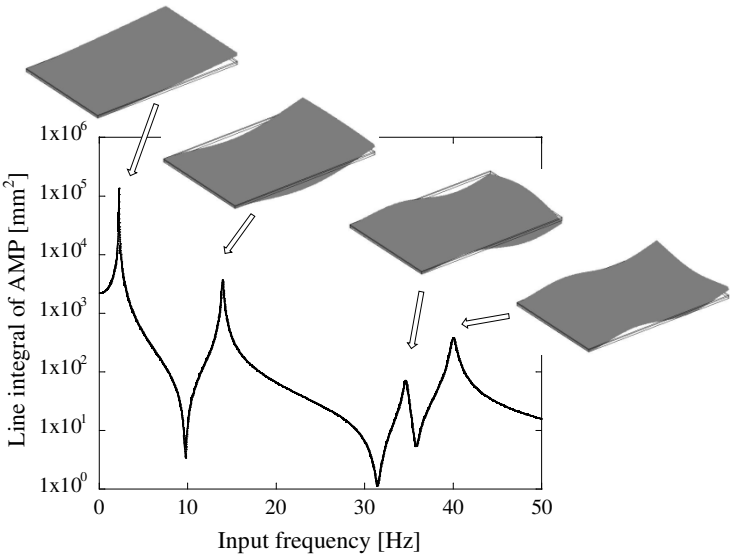

Figure 11: Frequency response and deformed shapes at resonance frequencies for the 3D FC structure with 0.01 Hz resolution. Gray solids show the deformed shapes while the lines indicate the original shapes.

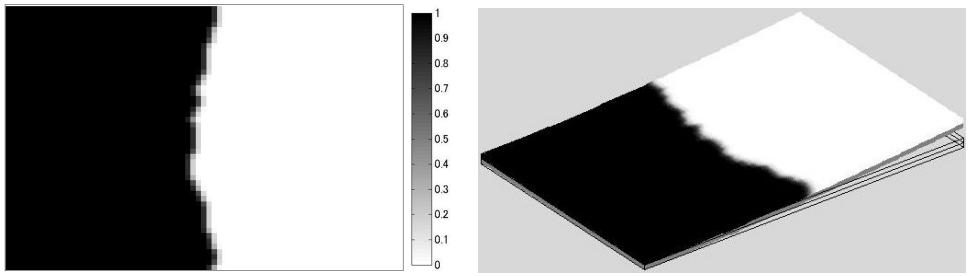

(a) (b)

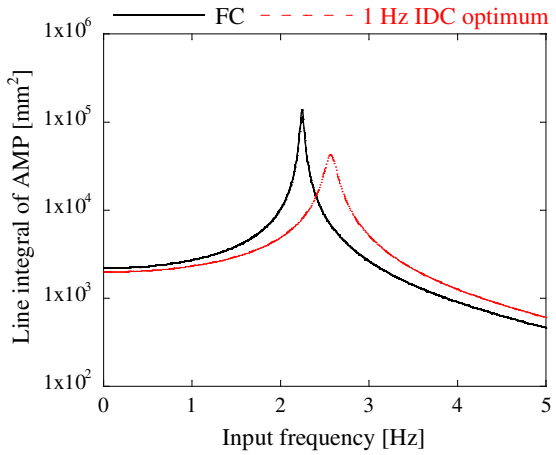

(c)

Figure 12: Optimal results for reducing the first mode resonance response. (a): Optimal configuration of the damping layer plotted by gray scale on the XY-plane. IDC was maximized under a 1 Hz excitation. (b): Deformed shape of the plate. Lines indicate original shapes. (c): Comparison of the line integration of AMP in the 0-5 Hz excitation frequency range with 0.01 Hz resolution.

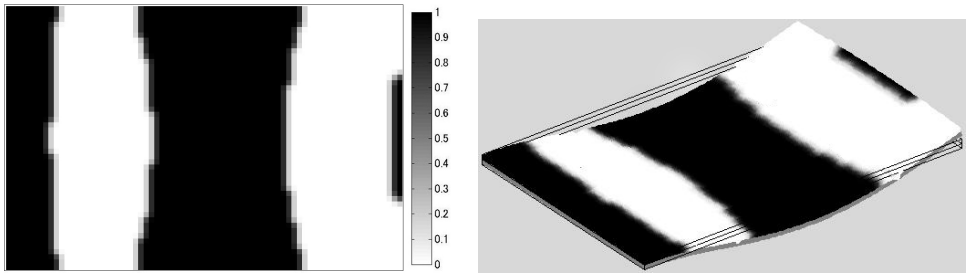

(a) (b)

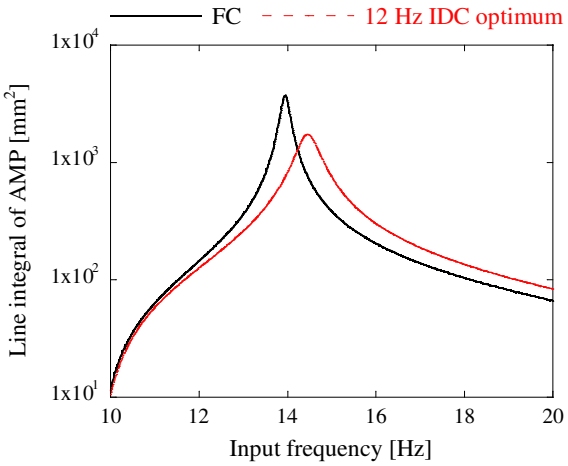

(c)

Figure 13: Optimal results for reducing the first mode resonance response. (a): Optimal configuration of the damping layer plotted by gray scale on the XY-plane. IDC was maximized under a 12 Hz excitation. (b): Deformed shape of the plate. Lines indicate original shapes. (c): Comparison of the line integration of AMP in the 10-20 Hz excitation frequency range with 0.01 Hz resolution.

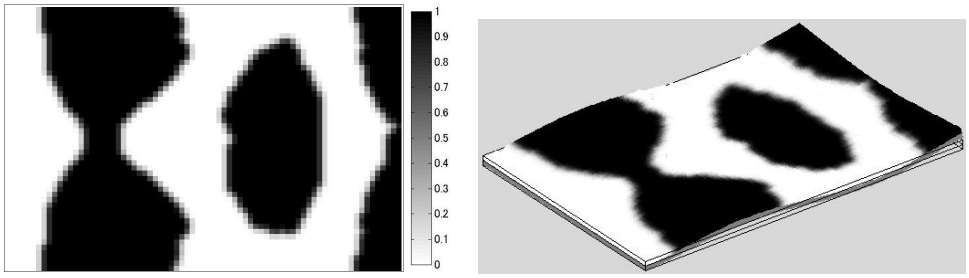

(a) (b)

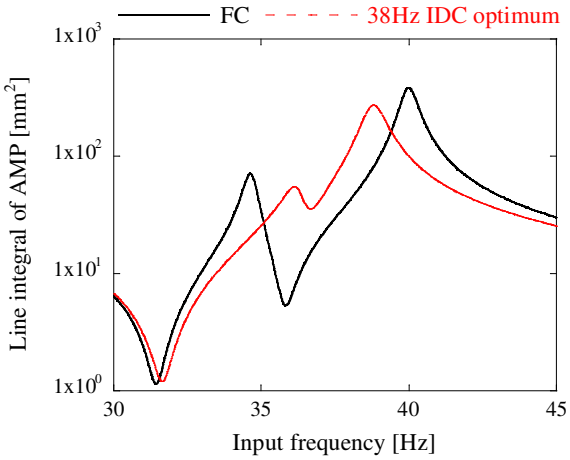

(c)

Figure 14: Optimal results for reducing the first mode resonance response. (a): Optimal configuration of the damping layer plotted by gray scale on the XY-plane. IDC was maximized under a 38 Hz excitation. (b): Deformed shape of the plate. Lines indicate original shapes. (c): Comparison of the line integration of AMP in the 30-45 Hz excitation frequency range with 0.01 Hz resolution.